Supplementary Information

to

Identifying Pitfalls when using the Miller-Abrahams Rate in Kinetic Monte Carlo Simulations

Magdalena S. Dörfler[1], Heinz Bässler[2], Andrey Kadashchuk[1], Harald Oberhofer[2] and Anna Köhler[1,2]*

[1] Soft Matter Optoelectronics, Experimental physics II, University of Bayreuth, Universitätsstraße 30, 95448 Bayreuth, Germany

[2] Bayreuth Institute of Macromolecular Research (BIMF), University of Bayreuth, Universitätsstraße 30, 95448 Bayreuth, Germany

[3] Chair for Theoretical Physics VII and Bavarian Center for Battery Technologies, University of Bayreuth, Universitätsstraße 30, 95448 Bayreuth, Germany

In memoriam I. I. Fishchuk († 2024)

A Simulation results with correlated disorder

In the following we show the results of simulations within a system with correlated disorder that were conducted in the same way and with the same parameters as the corresponding simulations with uncorrelated disorder in the main paper. To generate a system with correlated disorder, we use a method that was described by van der Holst et al [1]: The energy E_i at a site i is calculated from the electric fields of permanent dipoles at all other sites j within a correlation radius which we chose for all our simulations to be 25 nm. The relative distance between site i and j is given by the positional vector R_{ij}. All dipoles are randomly orientated but have the same strength $d = |d_j|$. The potential energy of a point charge at a site i is then given by

$$E_i = -\sum_{j \neq i} \frac{e d_j \cdot R_{ij}}{\epsilon_0 \epsilon_r |R_{ij}|^3},$$

Where e is the unit charge, ϵ_0 the vacuum permittivity, and ϵ_r the dielectric constant of the material.

The results obtained with correlated disorder are qualitatively similar to that of uncorrelated, albeit (i) the difference between using the full and the approximate rate is more pronounced and starts at higher disorder values, since correlated disorder implies a lower local disorder. (ii) The field dependence of the mobility shows a Poole-Frenkel-dependence ($\ln \mu \propto F$) down to lower field values.

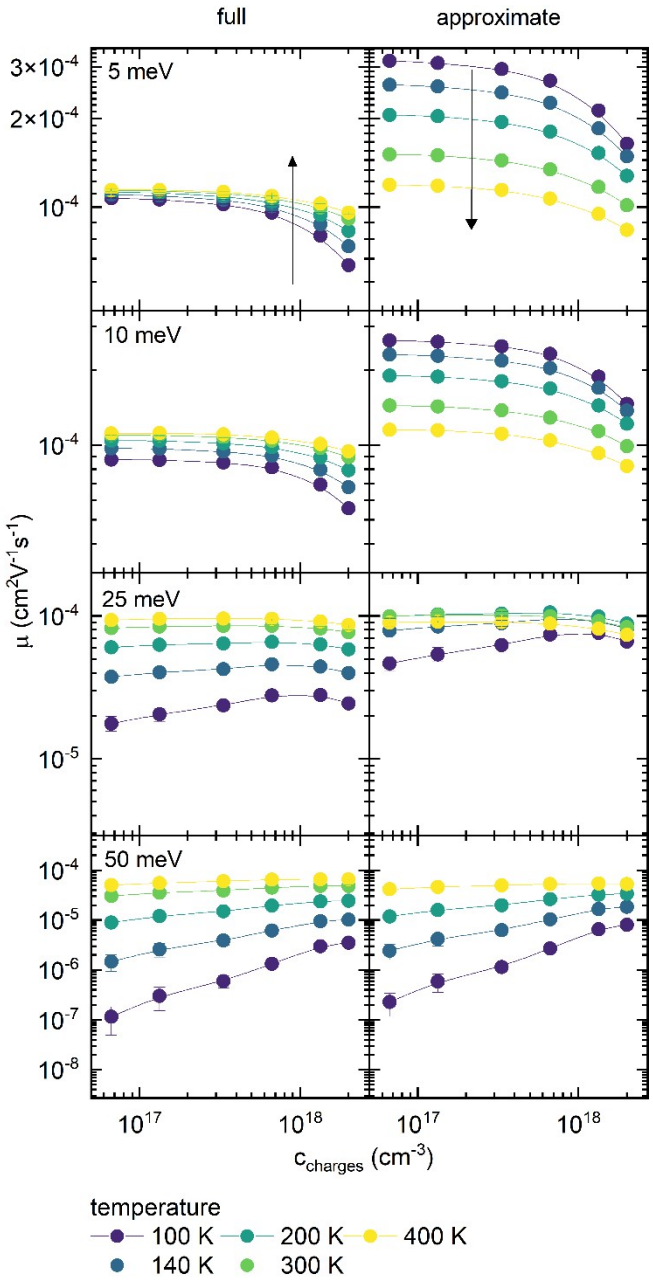

Figure S.1 Dependence of the carrier mobility on the gate voltage in an OFET geometry with correlated disorder, parametrized with different temperatures, shown for several disorder strength (from top to bottom: 5meV, 10meV, 25meV, 50meV), derived with the full rate (left-hand-side, μ_{full}) or the approximate rate (right-hand-side, μ_{approx}). The obtained results are similar to the results for uncorrelated disorder.

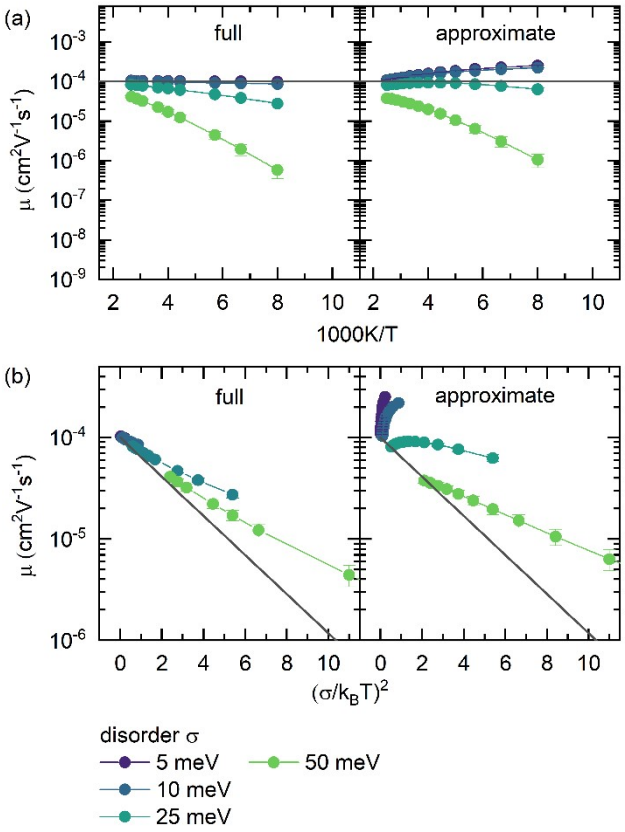

Figure S.2 Temperature dependence of the mobility in a system with correlated disorder for different σ = 50, 75,100 meV in an OLED-type device using either the full or the approximate MA rate. (a) Arrhenius representation. The auxiliary line at 10^{-4} cm²/(Vs) highlights the different temperature dependencies for 5 and 10 meV disorder for both rates. (b) Mobility plotted against the relative disorder $(\sigma/k_BT)^2$. The grey line shows an exponential decay with decay rate $(2/3)^2$. Beware that some data points pertaining to different values of σ might coincide. In contrast to the full rate, the results from the approximate rate depend on both T and σ differently, and at low disorders, the results from both rates differ greatly. At high mobilities, the confidence intervals are smaller than the symbol size.

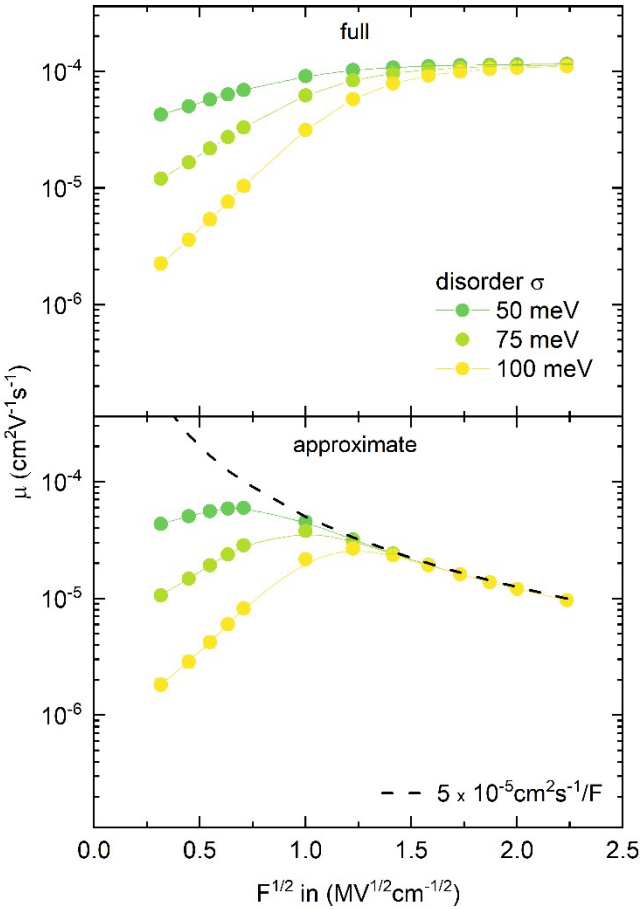

Figure S.3 Dependence of the mobility on the electric field in an OLED-type device at T=300K for the full (top) and approximate (bottom) Miller-Abrahams rate for correlated disorder. At low fields mobility increases with $\sqrt{F}$. At high fields the mobility saturates for the full rate while the mobility obtained from the approximate rate decreases 1/F (dashed line).

B Quantitative comparison of Mobility obtained from both rates

We show the ratio between the mobility calculated from both rates in Figure S.4. As can be seen, the mobility obtained by the approximate rate deviates from the mobility obtained by the full rate strongly. We especially want to point out, that even at high disorder strengths, the approximate rate leads to a mobility half as large as the full one.

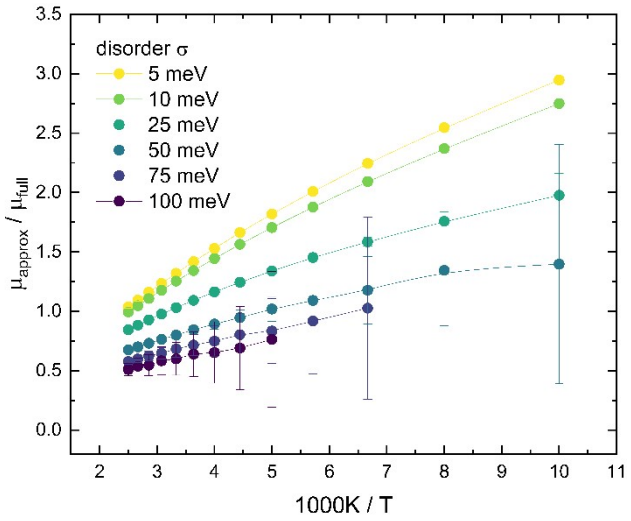

Figure S.4 Ratio between the mobility obtained with the approximate Miller-Abrahams rate to the one obtained with the full rate for the simulation data at different disorder strengths and temperatures of Figure 2 in the main paper.

C Mobility as a function of relative disorder over a broader value range

We show the mobility in a OLED-type device with random Gaussian disorder, as displayed in Figure 3 (b) of the main text, but extended over a wider range of relative disorder values $(\sigma/k_BT)^2$. Some data points coincide visually for different disorder strengths, particularly at low values of $(\sigma/k_BT)^2$. Therefore, the main text only presents an enlarged section of the same data for $(\sigma/k_BT)^2$ between 0.02 and 10.99 to highlight the differences between the two rates, especially at lower values of $(\sigma/k_BT)^2$. In Figure S.5, the relative disorder spans the following ranges for different disorder strengths: $(\sigma/k_BT)^2$ = 0.02–0.34 (5 meV), 0.08–1.35 (10 meV), 0.53–8.42 (25 meV), 2.10–21.55 (50 meV), 4.73–18.94 (75 meV), and 8.42–21.55 (100 meV). Analogous to Figure 3 (b), the grey line shows a decay $\mu \sim exp\left(-\left(\frac{2}{3}\cdot\frac{\sigma}{k_BT}\right)^2\right)$. As also explained in the main text, the deviation of the data points from this line at large values of $(\sigma/k_BT)^2$ arises from the finite size of the simulation box. Notably, this deviation additionally appears more pronounced due to the double-logarithmic scale.

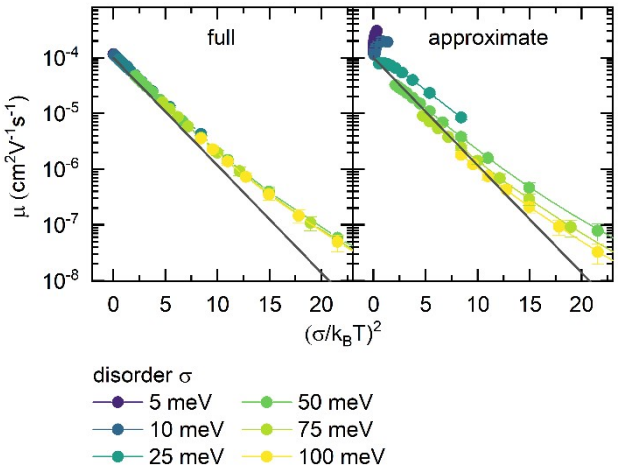

Figure S.5 Temperature dependence of the mobility for the full and the approximate Miller-Abrahams rate in a sandwich-type device. The mobility is plotted versus $(\sigma/k_BT)^2$, over a broader value range than in Figure 3 (b) in the main text. The grey line shows an exponential decay with a decay constant of $(2/3)^2$.

D Considering the rates within a more general formalism

Here we want to compare the full and the approximate rate within the more general formalism of Fornari et al. [4] to obtain a physical understanding of both. By assuming transition from state 1 to 2 promoted by electronic coupling, they derived the following rate expression:

$$k_{12} = \frac{\pi}{\hbar}\sum_m |M_{12,m}|^2\left[N\left(\omega_m^I\right)\rho_{FCWT}\left(\Delta E_{12} - \hbar\omega_m^I\right) + \left(N\left(\omega_m^I\right)+1\right)\rho_{FCWT}\left(\Delta E_{12} + \hbar\omega_m^I\right)\right. \quad \textbf{(1)}$$

The phonon modes m with energy ω_m^I modulate the coupling and induce the transition. $|M_{12,m}|^2$ is connected to the transition matrix element V_{12} by the displacement q_m via $V_{12} = |M_{12,m}|^2 q_m$. The phonon occupation number is given by $N\left(\omega_m^I\right) = \left(exp\left(\omega_m^I/k_BT\right) - 1\right)^{-1}$. ΔE_{12} is the energy difference between the lowest vibronic states of initial and final state, and ρ_{FCWT} is the density of states weighted with the Franck-Condon factor and temperature.

Fornary et al. [4] show that in absence of active accepting modes, only transitions at the resonance frequency can take place ($\omega = \omega'$) and ρ_{FCTW} becomes a δ-function. This is equal to the Marcus rate in the limit of vanishing reorganization energy and corresponds to non-local vibrational coupling [1]:

$$k_{12} = \frac{\pi}{\hbar}\sum_m |M_{12,m}|^2\left[N\left(\omega_m^I\right)\delta\left(\Delta E_{12} - \hbar\omega_m^I\right) + \left(N\left(\omega_m^I\right)+1\right)\delta\left(\Delta E_{12} + \hbar\omega_m^I\right)\right] \quad \textbf{(2)}$$

The derivation of the Miller-Abrahams rate considers charge transfer assisted by single-phonons with a continuous spectrum below the Debye-energy. By including those restrictions and introducing the spectral phonon density

$$J(\omega) = \sum_m |M_{12,m}|^2 \delta(\omega - \omega_m^I) \quad \textbf{(3)}$$

,

Fornari et al. [4] show that the conventional Miller-Abrahams transfer rate can be recovered. By performing a case distinction on (2), they find:

$$k_{12} = \begin{cases} \frac{\pi}{\hbar} J(-\Delta E_{12}/\hbar)\,\frac{exp(-\Delta E_{12}/k_BT)}{exp(-\Delta E_{12}/k_BT) - 1}, & for\ \Delta E_{12} < 0 \\ \frac{\pi}{\hbar} J(\Delta E_{12}/\hbar)\,\frac{1}{exp(\Delta E_{12}/k_BT) - 1}, & for\ \Delta E_{12} > 0 \end{cases} \quad \textbf{(4)}$$

The conventional Miller-Abrahams expression is recovered by choosing the spectral phonon density as [1]

$$J_{approx}(\pm\Delta E_{12}/\hbar) = \nu_0 \frac{\hbar}{\pi} e^{-2r\gamma} \cdot \frac{\exp(\pm\Delta E_{12}/k_BT) - 1}{exp(\pm\Delta E_{12}/k_BT)} \quad \textbf{(5)}$$

.

Here, we want to add that the full transfer rate we have considered in this paper is obtained by using a simpler expression for the spectral density, i.e.

$$J_{full}(\pm \Delta E_{12}/\hbar) = \frac{A}{\pi} e^{-2r\gamma} \cdot |\Delta E_{12}| \qquad \textbf{(6)}$$

Thus, the spectral density of the approximate rate converges towards a constant for large energy differences, while the spectral density of the full rate increases linearly (c.f. Figure S.5). That both spectral densities only agree for small ΔE_{12} seems on the first sight contradictory to the fact, that the approximate rate is obtained from the full rate in the limit of large energy differences $\Delta E_{12} \gg 2k_B T$. However, for obtaining the approximate rate, one additionally needs to introduce the attempt-to-hop frequency $\nu_0 = A/\hbar \cdot |\Delta E_{12}|$. Since this is usually chosen to be constant, both rates agree in the beforementioned limit. Therefore, within the framework of Fornari et al. [4], both rates are based on different assumptions for the spectral phonon density.

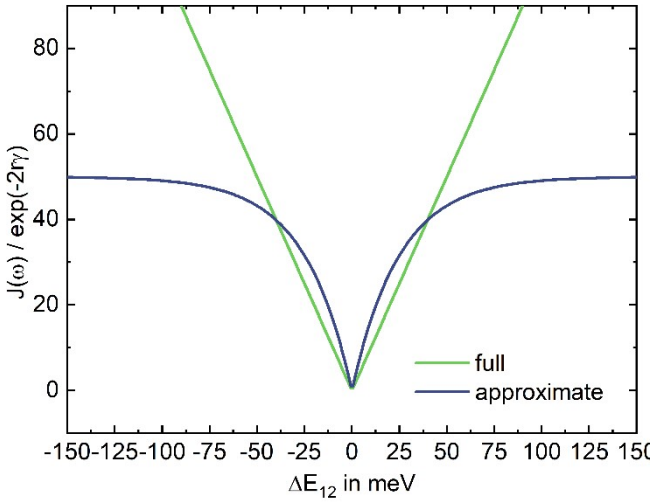

Figure S.6: Within the framework of a general hopping rate from the work of Fornari et al. [4] both the full and the approximate rate imply a certain spectral phonon density $J(\omega)$. The expressions for $J(\omega)$ one needs to assume to obtain both rates are given in the text and plotted here for the parameters $A/\pi = 1$, $\nu_0 \hbar/\pi = 1$, $k_B T =$ 25 meV (approx. room temperature). The prefactors A, ν_0 can be chosen arbitrarily; however, we found our chosen values allow a good visual comparison of the behavior of both functions.

E Relation of the diffusion coefficient and jump rate

Here, we show that the diffusion coefficient D depends linearly on the average hopping rate $\langle k \rangle$. For this, we follow the argumentation of Richard LeSar in *Introduction to Computational Materials Science* for diffusion with only nearest-neighbor hopping [2] and apply this to the case of the third-nearest-neighbor hopping we used in our simulations.

The diffusion coefficient D in 3d is connected to the mean square displacement $\langle R_n^2 \rangle$ over a timespan t:

$$D = \frac{1}{6t} \langle R_n^2 \rangle$$

In the following, we derive an expression for $\langle R_n^2 \rangle$. After n steps, the position of one of the considered particles is denoted as $R_n = r_1 + r_2 + ... + r_n$ with r_i being the positional change vector for the i^{th} step. The square displacement R_n^2 can therefore be written as:

$$R_n^2 = R_n \circ R_n$$

$$= (r_1 + r_2 + ... + r_n) \circ (r_1 + r_2 + ... + r_n)$$

$$= \sum_{k=1}^{n} r_k^2 + 2 \sum_{k=1}^{n-1} \sum_{j=k+1}^{n} r_k \circ r_j$$

Here, the first term summarizes over all $r_k \circ r_k$, while the second term summarizes $r_k \circ r_j$ where $k \neq j$. The last scalar product can also be written as $r_k r_j cos(\theta_{kj})$ with θ_{kj} being the angle between both vectors. Next, we take the average of the mean square displacement over several (all) trajectories n.

$$\langle R_n^2 \rangle = \left\langle \sum_{k=1}^{n} r_k^2 \right\rangle + 2 \left\langle \sum_{k=1}^{n-1} \sum_{j=k+1}^{n} r_k r_j cos(\theta_{kj}) \right\rangle$$

Let us first consider the second term. All steps over which we take the average are uncorrelated and for every step the chances to move left are the same to move right. This applies for all directions equally. Therefore, $\langle cos(\theta_{kj}) \rangle$ must be 0 and the second sum vanishes.

Now let us consider the first term. In agreement with our simulations, we will consider in the following jumps on a three-dimensional cubic grid to positions within the maximum hopping distance of $\sqrt{3}$a, therefore allowing hops up to the third-nearest-neighbor positions. By this, the average hopping distance d (with the zero vector as included possible hop) is in the case of our simulations given by

$$d = \frac{6 \cdot a + 12 \cdot \sqrt{2}a + 8 \cdot \sqrt{3}a + 1 \cdot 0}{27} = C \cdot a$$

With this, the mean square displacement after n hops can be written as

$$\langle R_n^2 \rangle = nC^2a^2.$$

The n hops occur with an average hopping rate $\langle k \rangle$ within an average time interval $\langle t \rangle$ with $n = \langle k \rangle \cdot \langle t \rangle$. With this, we finally arrive at an expression for the diffusion coefficient:

$$D = \frac{1}{6t} \langle R_n^2 \rangle = \frac{1}{6} C^2 a^2 \langle k \rangle$$

Therefore, the diffusion coefficient D depends linearly on the average hopping rate $\langle k \rangle$.

F Temperature dependence of the jump rates for varying energy differences

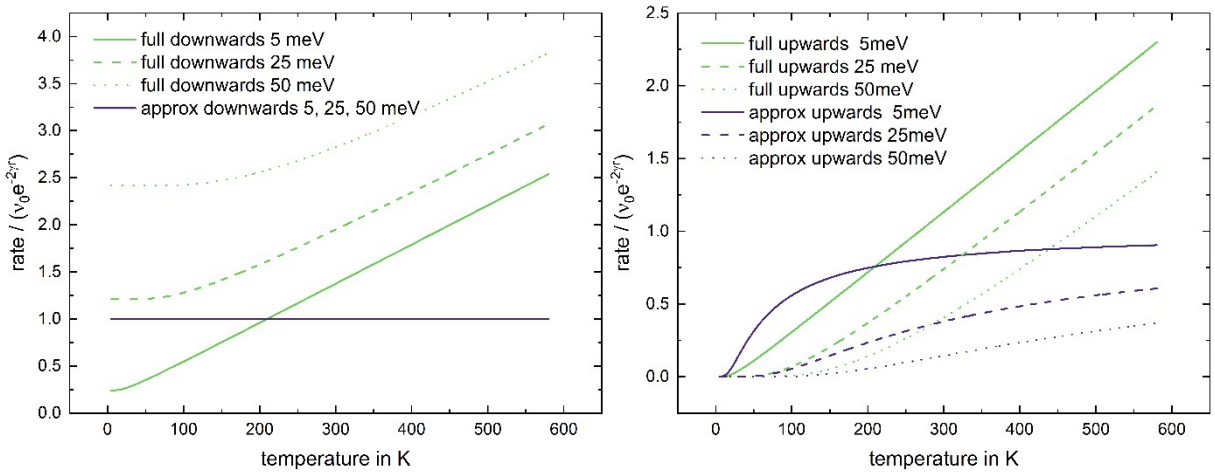

Figure S.7 Dependence of the full and approximate MA rates on the temperature for (left) downward hops and (right) upward hops. The full rate is shown in light green, the approximate in dark blue. Both rates are plotted for different values of the energy difference between initial and final state of the charge transfer. This energy difference is indicated via a solid, dashed or dotted line. For downward hops, the approximate rate does not depend on the energy difference, hence there is only a single line for all energy differences.

G Our criterion for high fields

Following Fishchuk et al. [3], we consider electrical fields F as strong, if $F \geq \sigma/ea$. Here, σ is the standard deviation of the energetic disorder with Gaussian shape, e the elementary charge and $a = 1nm$ the lattice constant.

σ [meV]	$F^* = \sigma/ea$ [MVcm^{-1}]	$\sqrt{F^*}$ [MV$^{1/2}$ cm$^{-1/2}$]
5	0.05	0.22
10	0.10	0.32
25	0.25	0.50
50	0.50	0.71
75	0.75	0.87
100	1.00	1.00

Table 1: Minimum field F^* for which $F \geq \sigma/ea$ is satisfied when the lattice constant is $a = 1nm$.

References

[1] J. J. M. van der Holst, F. W. A. van Oost, R. Coehoorn, and P. A. Bobbert, Monte Carlo study of charge transport in organic sandwich-type single-carrier devices, Phys. Rev. B **83**, 8 (2011).

[2] R. LeSar, *Introduction to Computational Materials Science: Fundamentals to Applications* (Cambridge University Press, Cambridge, 2013).

[3] I. I. Fishchuk, D. Hertel, H. Bässler, and A. K. Kadashchuk, Effective-medium theory of hopping charge-carrier transport in weakly disordered organic solids, Phys. Rev. B **65**, 125201 (2002).

[4] R. P. Fornari, J. Aragó, and A. Troisi, A very general rate expression for charge hopping in semiconducting polymers, The Journal of Chemical Physics **142**, 184105 (2015).